Instability Study of Oil Slicks Contained by A Single Boom

Jianzhi Fang, Kau-Fui Vincent Wong[†]
Department of Mechanical Engineering
University of Miami
Coral Gables, FL, USA
kwong@miami.edu

Abstract

In this fundamental study of two-layer (oil/water) flow past a vertical barrier (a single boom), the following factors are considered: gravity, surface tension, current velocity and depth, boom draft, oil viscosity and density. From the numerous simulations, it is predicted that in the cases with low oil viscosities, small-size vortices dominate in the oil slicks, which consume the kinetic energy transported from the water current and make the oil slicks more stable. In the cases with high oil viscosities, the large oscillations cause the oil slicks to become shorter and thicker. The oil-water interface shape is substantially influenced by the surface tension. However, surface tension may be negligible in the drainage failure and the critical accumulation failure. The depth of the water affects the oil containment significantly when the current depth is less than 10 times of the boom's draft. The stability of the oil slick movement is very sensitive to the Froude number. With the Froude number increasing, the coefficient of collected oil drops sharply at a certain Froude number, the critical value. This fact indicates that the Froude number is a very important parameter in studying oil boom problems. In the study of the effect of oil density, it is found that as an instability criterion, the critical reduced gravity is more appropriate than the critical Froude number.

[†] The author who is to receive correspondence.

Instability Study of Oil Slicks Contained by A Single Boom

Jianzhi Fang, Kau-Fui Vincent Wong[†]
Department of Mechanical Engineering
University of Miami
Coral Gables, FL, USA
kwong@miami.edu

1 Introduction

This problem comes from the oil spill contained by a single oil boom. Various hydrodynamic instabilities were observed in the water-oil-boom systems. In the literature, such instabilities are referred to as the boom containment failures, and three oil containment failures have been identified; they are entrainment failure, drainage failure, and critical accumulation failure (Cross and Hoult 1971, Leibovich 1976, Delvigne 1989). Oil and water are immiscible. They are usually separated by a distinct interface. Across the interface, the fluid density and viscosity change dramatically. Since the moving interface is highly coupled with the fluid flow, the location of the interface cannot be known in advance, and it becomes an important part of the solution of this hydrodynamic system. Among the numerical studies, Zalosh (1975, 1976) and Grilli, *et al.* (1996, 1997) modeled the interfaces as vortex sheets. Their studies are mainly concerned with entrainment failure. In another type of numerical studies, the flow fields are directly solved from the Navier-Stokes equations. The interfaces are then obtained from these flow fields (Milgram and Van Huoten 1978, Bai and Kim 1993, Clavelle and Rowe 1993). Clavelle and Rowe used the Volume of Fluids (VOF) method to convect and reconstruct the oil-water interface in an Eulerian frame. The VOF method has both of the advantages of Eulerian methods (handling the large interface deformation) and Lagrangrian

[†] The author who is to receive correspondence.

methods (maintaining the interface as a discontinuity). But owing to the coarse grid system, the low order VOF method used, and the lack of systematic calculations in their work, Clavelle and Rowe merely showed the promise of the VOF methods in studying oil spills. In this paper, the drainage failure and the critical accumulation failure are systematically studied. An advanced VOF (Volume of Fluid) algorithm (Fang and Wong 1999, Fang 2000) is applied to calculate the oil-water two layer flow. The surface tension is modeled by CSF (Continuum Surface Force) method (Brackbill, *et al.*, 1992).

2 Numerical Modeling

The following basic assumptions are made to model the oil-water flow.

1. Two-dimensional flow is assumed. Oil and water are Newtonian and incompressible. Their physical properties, such as density, viscosity and interfacial tension are constant. The temperature is unchanged over the simulations.
2. The volume fraction of oil is denoted by $f (0 \le f \le 1)$. The volume fraction is defined as the volume fraction of the oil in the computational cell.

$$f = \begin{cases} 0, \text{ (water)} \\ 0 < f < 1, \text{ (interface)} \\ 1, \text{ (oil)} \end{cases} \qquad (1)$$

Oil and water are immiscible, and they are separated by distinct interfaces. Across the oil-water interface, the velocity is continuous. The density r and viscosity m in a infinitesimal space element is modeled by the volume weighted functions, which are widely used in literature (Puckett and

Almgren, 1997).

$$\begin{cases} r = f \cdot r_{oil} + (1-f) \cdot r_{water} \\ m = f \cdot m_{oil} + (1-f) \cdot m_{water} \end{cases} \tag{2}$$

3. The calculation frame is shown in Fig. 1. The boom is fixed in this frame, the uniform flow U_0 is coming from the left side. The top boundary is a linearized free surface, and the bottom boundary is a rigid non-slip wall.

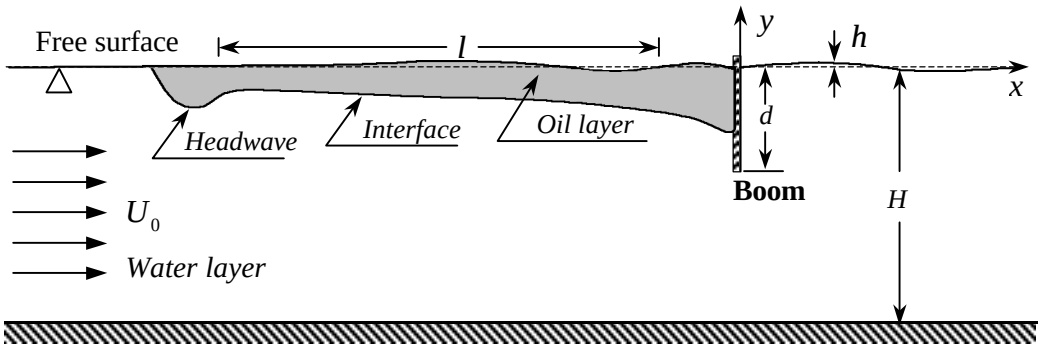

Figure 1 Modeling Configuration

The complete set of dimensionless governing equations are written as

$$\frac{\partial u}{\partial x} + \frac{\partial v}{\partial y} = 0 \tag{3}$$

$$r = (1-f) + f \cdot s_r \tag{4}$$

$$m = (1-f) + f \cdot s_m \tag{5}$$

$$\begin{aligned} &\frac{\partial (ru)}{\partial t} + \frac{\partial (ruu)}{\partial x} + \frac{\partial (ruv)}{\partial y} \\ &= -\frac{\partial p}{\partial x} + \frac{1}{\mathrm{Re}}\left[\frac{\partial}{\partial}\left(m\frac{\partial u}{\partial x}\right) + \frac{\partial}{\partial}\left(m\frac{\partial u}{\partial y}\right)\right] + \frac{2}{We} kf \frac{\partial f}{\partial x} \end{aligned} \tag{6}$$

$$\frac{\partial(rv)}{\partial t}+\frac{\partial(rvu)}{\partial x}+\frac{\partial(rvv)}{\partial y}$$
$$=-\frac{\partial p}{\partial y}+\frac{1}{\mathrm{Re}}\left[\frac{\partial}{\partial}\left(m\frac{\partial v}{\partial x}\right)+\frac{\partial}{\partial}\left(m\frac{\partial v}{\partial y}\right)\right]+\frac{2}{We}kf\frac{\partial f}{\partial y}-\frac{r}{Fr^2} \tag{7}$$

$$\frac{\partial f}{\partial t}+u\frac{\partial f}{\partial x}+v\frac{\partial f}{\partial y}=0 \tag{8}$$

where the important dimensionless numbers in this study are

$$\mathrm{Re}=\frac{r_{\mathrm{water}}U_0 d}{m_{\mathrm{water}}}\text{, Reynolds number} \tag{9}$$

$$\mathrm{Fr}=\frac{U_0}{\sqrt{gd}}\text{, Froude number} \tag{10}$$

$$\mathrm{We}=\frac{r_{\mathrm{water}}U_0^2 d}{s}\text{, Weber number} \tag{11}$$

$$s_r=\frac{r_{\mathrm{oil}}}{r_{\mathrm{water}}}\text{, Oil relative density} \tag{12}$$

$$s_m=\frac{m_{\mathrm{oil}}}{m_{\mathrm{water}}}\text{, Oil relative viscosity} \tag{13}$$

$$h_d=H/d\text{, Depth ratio} \tag{14}$$

Dimensionless time is scaled by d/U_0. s is the oil/water interfacial tension coefficient, k is the curvature of the interface. Modeled by CSF (Brackbill, *et al.*, 1992), the curvature k is expressed as

$$k=-\nabla\cdot\hat{\mathbf{n}}=\frac{1}{|\mathbf{n}|}\left[\left(\frac{\mathbf{n}}{|\mathbf{n}|}\cdot\nabla\right)|\mathbf{n}|-(\nabla\cdot\mathbf{n})\right] \tag{15}$$

where $\hat{\mathbf{n}}=\mathbf{n}/|\mathbf{n}|, \mathbf{n}=\nabla f$.

The domain of this study is a rectangular region. On the sides of this rectangle,

the boundary conditions are given below. The upstream incoming flow is assumed uniform.

$$\begin{cases} u = 1 \\ v = 0 \end{cases} \quad \text{at } x \to -\infty \tag{16}$$

At the other end, considered to be far downstream, the flow is fully developed along the horizontal direction.

$$\frac{\partial u}{\partial x} = \frac{\partial v}{\partial x} = 0 \qquad \text{at } x \to +\infty \tag{17}$$

The bottom boundary is approximated as a rigid no-slip wall,

$$u = v = 0 \qquad \text{at } y = -h_d \tag{18}$$

On the free surface, it is assumed that the elevation h over the level $y = 0$ is very small compared to the surface wavelength ($h << l$) and the boom draft ($h << d$). So it is appropriate to assume that $\frac{\partial h}{\partial x} \approx 0$, and the unit vector which is normal to the free surface pointing out of the fluid domain is (0, 1). Then the kinematic boundary condition $D(h - y)/Dt = 0$ at $y = 0$ can be written as

$$\frac{\partial h}{\partial t} + u\frac{\partial h}{\partial x} - v = 0 \quad \Rightarrow \quad \frac{\partial h}{\partial t} \approx v \tag{19}$$

The continuity of normal and tangential stresses at the linearized free surface leads to the dynamic boundary conditions. In the normal direction,

$$\left(-p + rgh + 2m\frac{\partial v}{\partial y} - s_0 \frac{\partial^2 h}{\partial x^2} \right)_{y=0} = 0 \tag{20}$$

where s_0 is the air/water or air/oil interface coefficient. If we neglect the interfacial

tension on the free surface, Eqn. (20) becomes,

$$\left(-p + rgh + 2m\frac{\partial v}{\partial y} \right)_{y=0} = 0 \qquad (21)$$

In the tangential direction,

$$m\left(\frac{\partial u}{\partial y} + \frac{\partial v}{\partial x} \right)_{y=0} = 0 \qquad (22)$$

The linearized free surface condition assumes the surface elevation is very small and only important in calculating the velocity and pressure, but the mesh maintains a rectangular geometry. This limits its use to simulate wave surface condition.

With a given volume fraction field, any control-volume based N-S solver can be used to calculate the pressure and velocities by solving Eqns. (3)-(7). In order to minimize numerical dispersion, the volume fraction equation is solved separately by applying the VOF method. Instead of direct discretization of Eqn. (8), in the VOF method two steps are taken to calculate the volume fraction field. The first step is to reconstruct the geometry of the water-oil interface from the volume fraction field. The second step is to convect the volume fraction field based on the velocity field and the reconstructed interface. The detail description of the VOF method used in this study is described in Fang and Wong (1999).

The numerical model has been tested extensively. Two of the validation cases are presented below. The first case is the multi-layer flow past a vertical barrier. This case is similar to the experiment in which the trace ink is used to visualize the streamlines. The upstream condition has three dark-fluid layers flowing in; each layer is four-cell wide at the entrance. The flow is made to pass by a vertical barrier. By

allowing the two fluids to have the same physical properties (viscosity and density) and zero interfacial tension at the interface, the dark fluid should act as perfect trace ink that does not disturb the flow field. As presented in Fig. 2, the dark fluid layers do not show visible dispersion and are confined within their streamlines, as they should be.

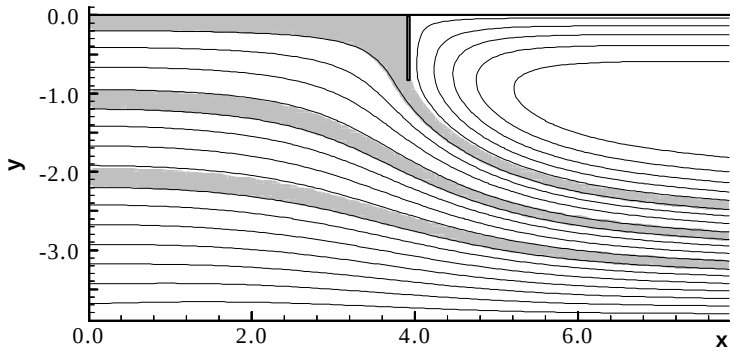

Figure 2 Multi-layer flow past a vertical barrier (Re=5000)

The second case is the interface evolution under the influence of interfacial tension. In the absence of gravity and other external forces, a static liquid drop of any arbitrary shape will become spherical under the influence of the interfacial tension. In the two-dimensional case, a liquid block of any shape should eventually evolve into a circular shape. Across the circular surface, there should be a jump in the fluid pressure of magnitude (Batchelor, 1973)

$$\Delta p = \frac{s}{R} \tag{23}$$

where R is the radius of the circle. In this test case, the initial shape of the dark fluid is given as a square. A 100×100 mesh presents the entire computational domain (2.5×2.5, the side dimension of the dark-fluid block is 1 at the initial time) with

uniform mesh spacing $\Delta x = \Delta y = 0.025$. Assume that the fluids are incompressible, then the dimensionless radius R of the final dark-fluid circle can be calculated by the mass conservation,

$$pR^2 = 1 \times 1 = 1 \quad \Rightarrow \quad R = 1/\sqrt{p} \tag{24}$$

Suppose the density ratio $s_r = 1$, the gravity thus has no effect on the dark fluid. The other dimensionless parameters are given as $\mathrm{We} = 1$, $\mathrm{Re} = 100$, and $s_m = 1$. The dimensionless form of Eqn. (23) gives the theoretical pressure jump as

$$\Delta p = \frac{1}{\mathrm{We} \cdot R} = \sqrt{p} \approx 1.772 \tag{25}$$

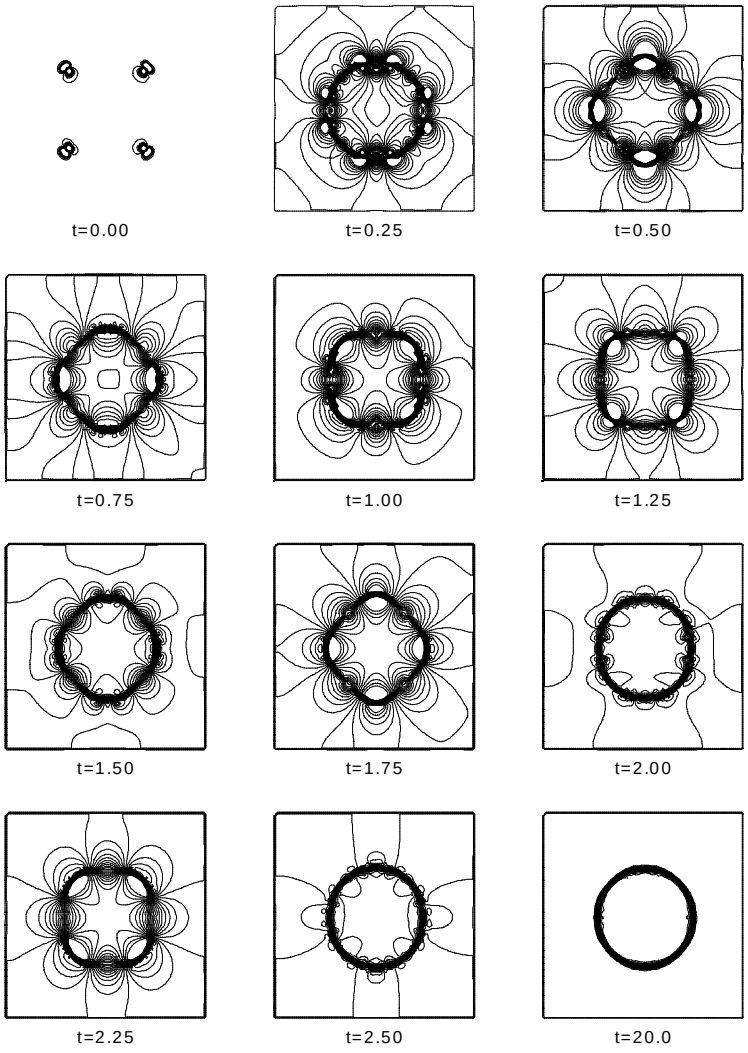

Figure 3 Pressure contour plots

The pressure contour plots are tabulated in Fig. 3. All the pressure contour plots are using the same contour levels: in the range between -1.8 and 1.8, the pressure magnitude is presented in the form of nineteen pressure contours with equal increments of 0.2. To compare the calculated pressure jump with theoretical prediction, a mean dark-fluid pressure is calculated from the cells where the dark fluid volume fraction $f \geq 0.99$. At $t = 20$, the pressure field is almost uniform both inside and outside the dark-fluid circle (Fig. 3), and the calculated pressure jump is $\Delta p = 1.761$. Compared with the theoretical prediction of Eqn. (25), there is only a 0.7% relative error.

3 Numerical Study Scheme

In the study of oil containment by a single oil boom, Fang (2000) collected data from the available references, and found that the dimensionless parameters fall into the following ranges: $s_r \in [0.8, 0.95]$, $s_m \in [10^0, 10^4]$, $\mathrm{Fr} \in [0.02, 1.2]$, $\mathrm{Re} \in [10^2, 10^5]$, $\mathrm{We} \in [10^1, 10^5]$ and $h_d \in [1.5, 10]$. An exhaustive investigation of the parameter space $\{s_r, s_m, \mathrm{Re}, \mathrm{Fr}, \mathrm{We}, h_d\}$ is beyond the scope of the present study. Rather a selected range of these parameters is considered that are appropriate for case studies. In Table 1 is listed the selected parameter sets for the present numerical study. Five experimental groups are designed to study the influences of the five dimensionless parameters $s_r, s_m, \mathrm{Re}, \mathrm{We},$ and h_d.

In addition, most of the groups have two subgroups. The parameters in the first subgroup are designed to simulate the general laboratory experimental conditions, it

will be called the first parameter set, denoted by $\Re_1$; while the parameters in the second subgroup are close to the real oil-slick containment conditions, it will be called the second parameter set, denoted by $\Re_2$. A parameter set in this paper refers to a set that contains all the modeling parameters to describe an oil containment condition. The oil used in the laboratory studies is usually light oil, which has lower density and less viscosity than the real spilled oil has. In Table 1, the oil relative densities are assigned 0.85 and 0.90, and the oil relative viscosities are assigned 10 and 1000 for the first and the second parameter set, respectively. The other three parameters, namely the depth ratio, the Reynolds number and the Weber number, are correspondingly assigned 2.5, 1000, 100 and 10, 5000, 1000. So $\Re_1$ and $\Re_2$ have been assigned as

$$\begin{aligned} \Re_1 &= \{s_m(10.0),\, s_r(0.85),\, h_d(2.5),\, \mathrm{Re}(1000),\, \mathrm{We}(100),\, \mathrm{Fr}\} \\ \Re_2 &= \{s_m(1000),\, s_r(0.90),\, h_d(10),\, \mathrm{Re}(5000),\, \mathrm{We}(5000),\, \mathrm{Fr}\} \end{aligned} \tag{26}$$

In the simulations, the oil slick is initially placed at the upstream side as a rectangular block (see Fig. 1), with 3 cells deep by 140 cells wide. At $t = 0$, the incoming flow velocity U_0 is linearly increased from 0 to the maximum dimensionless value 1 over a short time of dimensionless time period 1. Because the change in elevation of the free surface is assumed to be very small, the whole computational domain is maintained as a rectangular region during the simulation. The computational domain is discretized by a mesh that consists of 400×80 (horizontal by vertical) control volumes with non-uniform grid sizes. The adequacy of this fine grid was examined by performing calculation with a coarse grid containing half as many control volumes in each direction, that is 200×40 cells. The

two meshes give nearly the same solution. Meshes that are finer than 400×80 grids were not considered in this study due to the long computational time. Thirty-four computers (Pentium II 400 PC) were used to perform the calculations. For a typical case, the computation time is about 15 hours on a single computer.

Table 1 Dimensionless Parameters for Case Study

<table>
<tr><th rowspan="2">Group</th><th colspan="6">Parameters</th></tr>
<tr><th>s_m</th><th>s_r</th><th>h_d</th><th>Re</th><th>We</th><th>Fr</th></tr>
<tr><td rowspan="2">Group-s_m</td><td rowspan="2">1,10,100
1000
10000</td><td>0.85</td><td>2.5</td><td>1000</td><td>100</td><td rowspan="8">Fr is determined during the simulations.</td></tr>
<tr><td>0.90</td><td>10.0</td><td>5000</td><td>5000</td></tr>
<tr><td rowspan="2">Group-We</td><td>10</td><td>0.85</td><td>2.5</td><td>1000</td><td rowspan="2">50, 500
5000
infinite</td></tr>
<tr><td>1000</td><td>0.90</td><td>10.0</td><td>5000</td></tr>
<tr><td rowspan="2">Group-h_d</td><td>10</td><td>0.85</td><td rowspan="2">1.5, 2.0
2.5, 5.0
7.5,10.0</td><td>1000</td><td>100</td></tr>
<tr><td>1000</td><td>0.90</td><td>5000</td><td>5000</td></tr>
<tr><td rowspan="2">Group-s_r</td><td>10</td><td rowspan="2">0.8,0.85
0.9,0.95</td><td>2.5</td><td>1000</td><td>100</td></tr>
<tr><td>1000</td><td>10.0</td><td>5000</td><td>5000</td></tr>
<tr><td>Group-Re</td><td>10</td><td>0.85</td><td>2.5</td><td>10^2 - 10^5</td><td>100</td></tr>
</table>

4 Numerical Results

In this section, we will present the numerical results of the cases listed in Table 1. Basically, two types of results are presented: one is the characteristic of the interface movement; another is the coefficient of collected oil and the critical containment conditions. All the parameters in this section are dimensionless. Their definitions have been given in Eqns. (9)-(14), except that the coefficient of collected oil is defined here by

$$V_{\text{oil}} = \frac{\text{Volume of the Collected Oil at Steady State}}{\text{Volume of the Total Oil at Initial State}} \tag{27}$$

The coefficient of collected oil will be used to measure the oil boom performance under a given parameter set $\Re$ ($\Re = \Re_1, \Re_2$). Subset $\Re \setminus \{\text{Fr}\} = \{\text{Re}, \text{We}, s_m, s_r, h_d\}$ is directly selected from Table 1, where the forward slash in $\Re \setminus \{\text{Fr}\}$ means to subtract the subset $\{\text{Fr}\}$ from the set $\Re$. The Froude number is determined during the simulations. First, four calculations are performed under a given subset $\Re \setminus \{\text{Fr}\}$, and four Froude numbers that are sampled equidistantly over a reasonable large range. Second, the values of V_{oil} obtained from the previous calculations are checked; the values of V_{oil} may have a large drop between two simulation cases with the adjacent Froude numbers. More Froude numbers are then inserted between these two adjacent Froude numbers for further calculations. It may be necessary to repeat the second step in order to capture the drop of V_{oil}. In other words, the critical containment condition may be obtained by adjusting the Froude number.

4.1 Effect of the Oil Relative Viscosity

In the studies of the oil slick contained by an oil boom, the effect of the oil

viscosity was rarely discussed. Only Delvigne (1989) and Johnston, *et al.* (1993) addressed this topic in their experimental studies and found under certain conditions, a large-scale oscillation of movement may occur in a highly viscous oil slick ($s_m > 3000$), which may result in the critical accumulation failure. In this section, over 400 simulation cases have been carried out for the purpose of investigating the effect of the oil viscosity on oil containment by a single boom.

The movement of oil slicks with low oil relative viscosity ($s_m = 10$) is shown in Fig. 4. The simulation parameters are given by $\Re_1$ with Fr = 0.24 for this case. In each of the time-series frames, the dark layer is the oil slick. The horizontal line on the top of the oil slick is the free surface, and the vertical line on the right side of the oil slick represents the oil boom.

It is seen in frame Time=1 and frame Time=3 that the oil slick is stretching out along the free surface and becoming longer and longer before the oil slick reaches the oil boom. This movement is partially due to the buoyancy force. At Time=5, the oil slick has reached the oil boom. From the frame Time=7, it is seen that the oil begins to escape just under the skirt of the boom. At Time=13, a crest is forming near the oil boom and then moves backward. After Time=35, no more oil escapes, the movement of the oil slick reaches a pseudo-steady state, the headwave is seen at the leading edge of the slick.. In this case, about 70% of the initial oil has been entrapped by the oil boom, $V_{\text{oil}} \approx 0.7$.

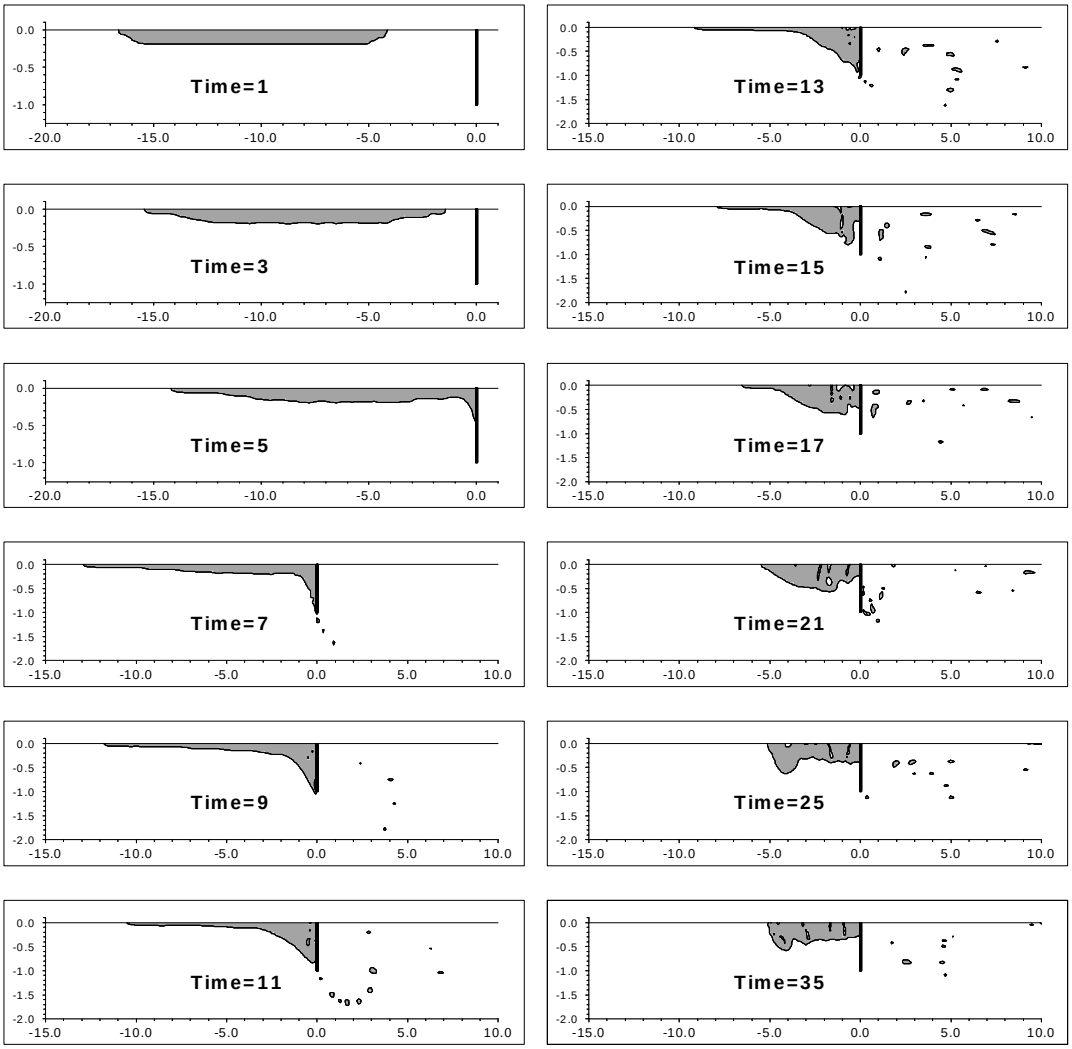

Figure 4 Evolution of the low viscous oil slick

The evolution of oil slicks with high oil relative viscosity ($s_m = 10{,}000$) is shown in Fig. 5. The physical parameters are $\Re_2$ with Fr = 0.16. In this case, the slicks move much slower compared to the previous case. An interesting result is that the large oscillations observed in the experiments of highly viscous slicks (Delvigne, 1989) are found in the present simulations. As shown in Fig. 5, before the slick reaches the boom, the left side of the oil slick is thicker than the right side (frame Time=10). This is the natural pattern of a highly viscous oil slick floating on the

current without any barriers, because the movement inside the slick is decreased quickly due to the high viscosity. After the slick reaches the boom, it continues to move forward due to inertia. At Time=30, the right side of the slick is thicker than its left side. While during Time=30 to Time=50, the thickest point of the slick moves back from the right side to the left side. This periodic movement continues, then the oil slick becomes shorter and shorter.

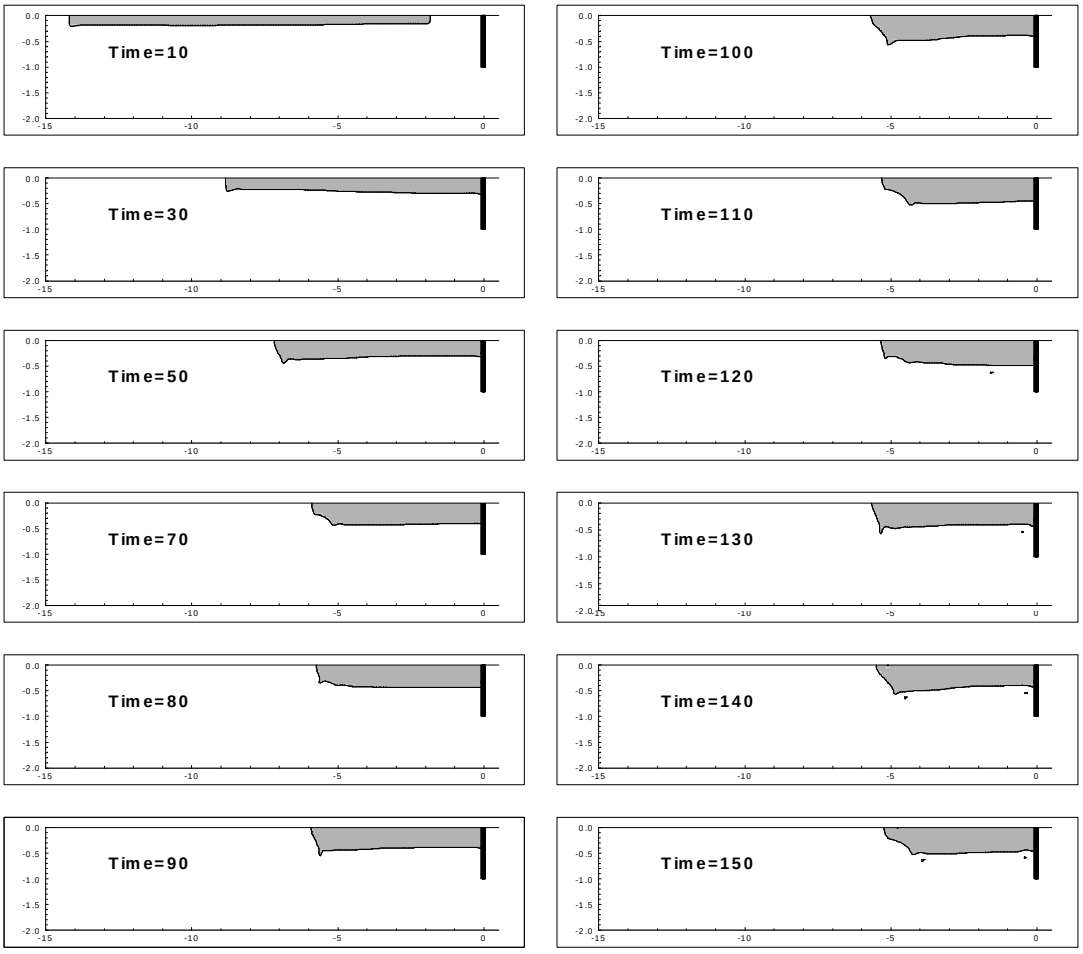

Figure 5 Evolution of the highly viscous oil slick

In order to understand the periodic movement, eight frames in Fig. 5 were enlarged and plotted with the corresponding velocity vectors and streamlines around

the slick (Fig. 6). In Fig. 6, it may be appropriate to consider that the frames from Time=70 to Time=100 represent one oscillation period and the frames from Time=110 to Time=140 represent another. At the beginning of the first period, the oil slick is moving forward to the oil boom and the slick on the side near the boom is becoming thicker. But the buoyancy counters this movement, a strong vortex just under the oil slick has formed in the counterclockwise direction (frame Time=70). This vortex forces the slick to move backward in the opposite direction against the current. In frame Time=80, a vortex is found around the leading edge, the leading edge begins to move downward, and a headwave is quickly established (frame Time=90). The formation of the headwave increases the effective area where the current pushes the oil slick forward. Finally, the oil slick follows the current, moves forward again. The headwave becomes flatter and smoother (frame Time=100). At Time=110, the discussed oscillation has finished, the length of the oil slick has become shorter about 0.21d during this oscillation period. At the end of the oscillation, the next cycle begins. In the two cycles shown in Fig. 6, the flow patterns are very similar to each other. But after each oscillation, the slick becomes shorter and thicker.

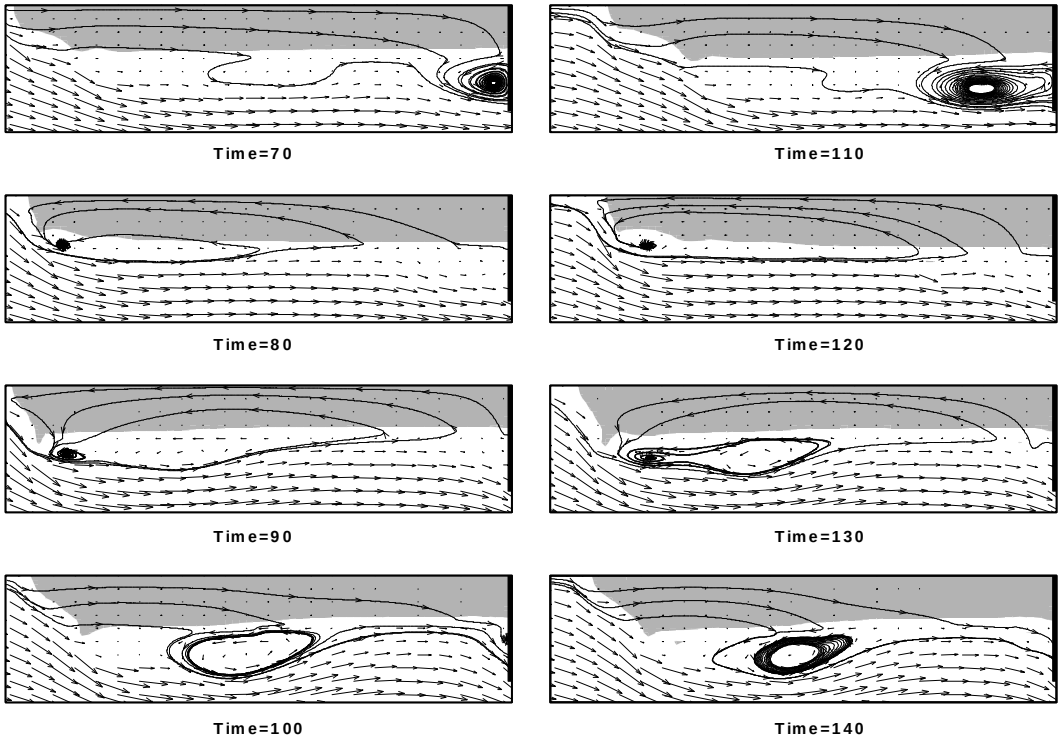

Figure 6 Velocity vector and Streamline plots

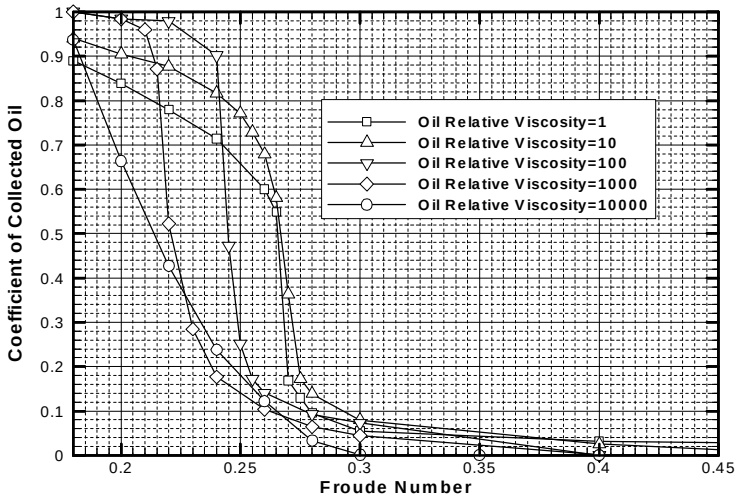

Figure 7 Effect of the oil relative viscosity (the first parameter set)

In Figures 7 and 8, every point comes from a unique calculation case. In the

cases presented in Fig. 7, the simulation parameters are chosen from the first parameter set $\Re_1$, while in Fig. 8, the parameters are chosen from $\Re_2$. It is noticed that the coefficient of collected oil drops sharply at a certain Froude number for each parameter set $\Re$. We define this Froude number as the critical Froude number under the given condition $\Re$, and assign it the symbol $F_{cr}^{\Re}$. When the Froude number exceeds $F_{cr}^{\Re}$, significant oil begins to escape. Another interesting observation to make regarding the results shown in Figures 7 and 8 is that when the oil relative viscosity is as low as 1 to 10, a significant amount of oil has been lost when the Froude number is much smaller that the critical Froude number.

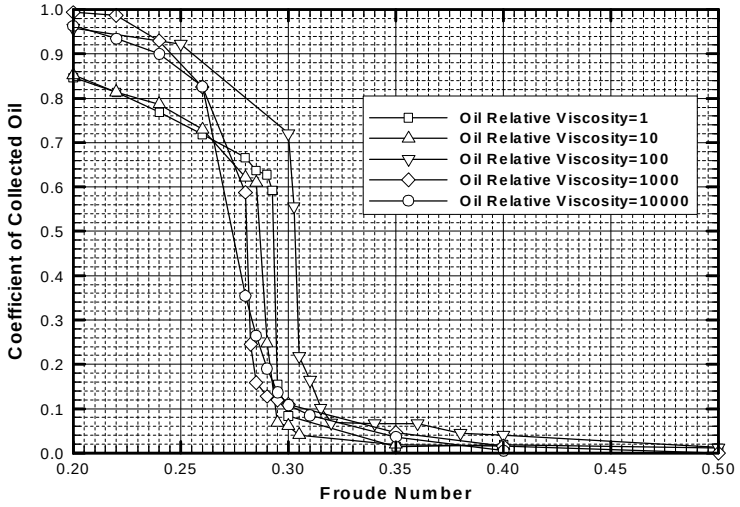

Figure 8 Effect of the oil relative viscosity (the second parameter set)

To investigate the influence of the oil viscosity, about 200 cases with 17 different oil relative viscosities were selected from the range of $10^0 \le S_m \le 10^4$, and 17 critical Froude numbers were then obtained. The parameter set $\Re_2 \setminus \{s_m\}$ is chosen to simulate the full-scale oil-spill situation. The relationship between S_m and

the critical Froude number $F_{cr}^{\Re_2 \setminus \{s_m\}+\{S_m\}}$ is shown in Fig. 9. At the beginning ($S_m = 1$), $F_{cr}^{\Re_2 \setminus \{s_m\}+\{S_m\}}$ decreases when S_m increases. Once $F_{cr}^{\Re_2 \setminus \{s_m\}+\{S_m\}}$ reaches its first local minimum value around $S_m \approx 17.8$, $F_{cr}^{\Re_2 \setminus \{s_m\}+\{S_m\}}$ begins to increase until it reaches its absolute maximum around $S_m = 100$. After that point, the $F_{cr}^{\Re_2 \setminus \{s_m\}+\{S_m\}}$ decreases monotonically over the range of $10^2 \le S_m \le 10^4$.

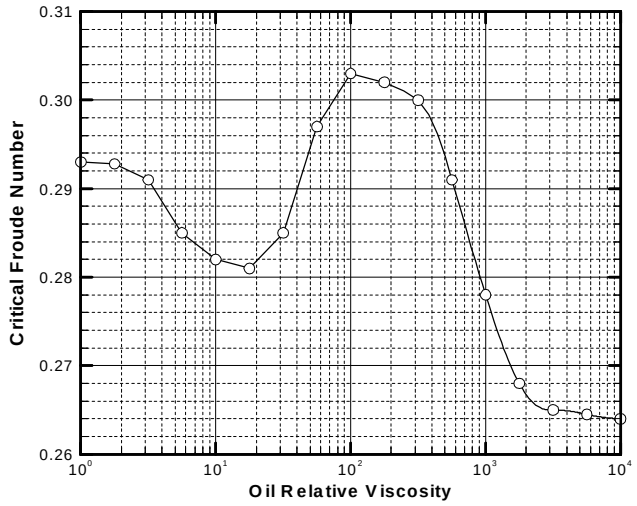

Figure 9 Oil relative viscosity vs. the critical Froude number

In Fig. 10, four streamline plots snapshot four steady-state solutions with parameter set $\Re_1 \setminus \{s_m\} + \{S_m\}$, where $S_m \in \{10^1, 10^2, 10^3, 10^4\}$. In the first three cases, the Froude numbers are the same, $\mathrm{Fr} = 0.22$; while in the last one with $S_m = 10^4$, $\mathrm{Fr} = 0.18$. Because $F_{cr}^{\Re_1 \setminus \{s_m\}+\{S_m = 10^4\}} < 0.22$, at $\mathrm{Fr} = 0.22$ most of the oil escapes and there is no visible slick at steady state for the last simulation case. By scrutinizing the streamline plots presented in Fig. 10, an attempt to partially explain some of the aforementioned results will be made. The first observation is that when the viscosity

becomes larger, the number of the vortices inside the slick decreases, and the vortex strength becomes weaker because of the decrease in the oil-slick velocity. In case (d) with $S_m = 10^4$, no vortex is actually found in the slick. From the viewpoint of energy conservation, when the energy is transferred into the oil slick from the current, the slick may not follow the current only if there is a mechanism, such as the vortex, to completely consume this energy. Otherwise, the slick must move to convert the input into its kinetic energy, and overcome buoyancy to accumulate it as gravitational potential energy. This movement and accumulation may eventually cause the boom to fail at a smaller Froude number, compared to low viscous slicks, which are dominated by the vortices.

On the other hand, when the viscosity is lower, the slick is longer and the vortices inside the slick are stronger. Then there is a greater chance for the oil and water to be mixed by the stronger vortices over the longer interface. If oil is mixed with water and enters the underflow current, this part of the oil may easily be washed away, just like the oil droplets in Kelvin-Helmholtz instability. This may be the reason for the low viscous slick ($S_m = 1, 10$) losing a significant amount of oil even when Froude number is much smaller than its critical Froude number.

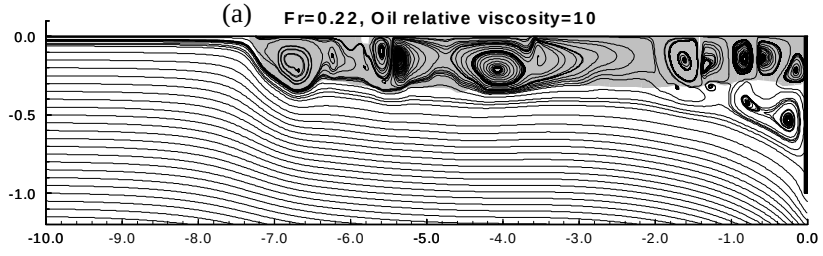

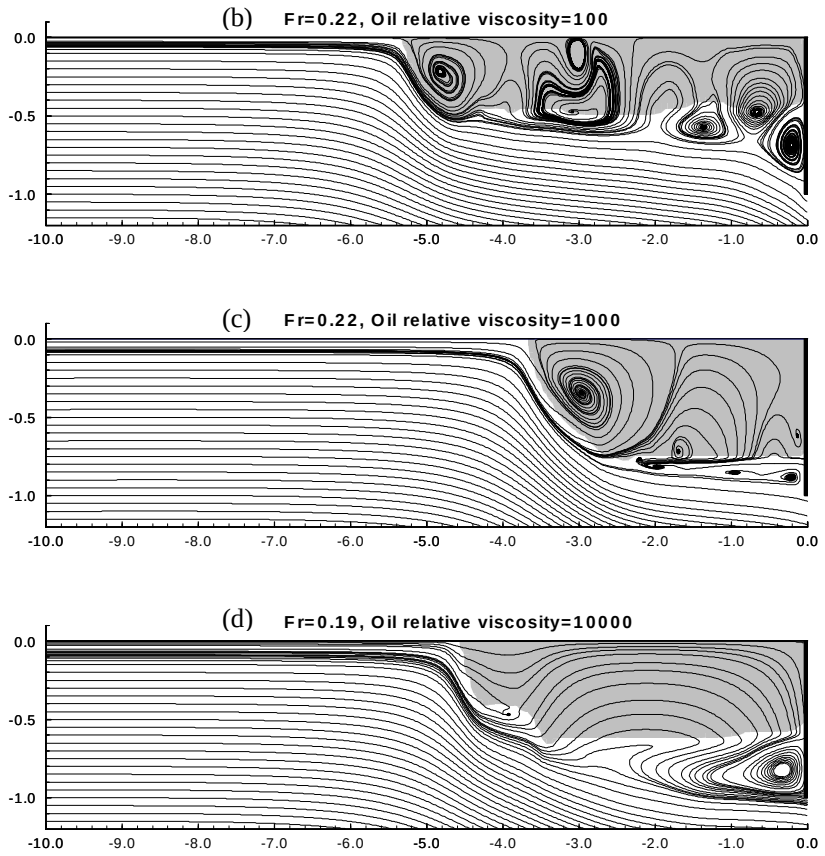

Figure 10 Streamlines around the different viscous oil slicks

4.2 Effect of the Weber Number

It is known that the interfacial tension has the effect of weakening the instability in the Kelvin-Helmholtz type. However, in drainage failure and critical accumulation failure, the effect of the interfacial tension is rarely studied. In order to reveal how the interfacial tension contributes to these two failures, four Weber numbers over a large range--which are equal to 50, 500, 5000 and ∞--have been investigated. In the case with the Weber number of infinity, $\mathrm{We} = 1.0 \times 10^{30}$ is actually assigned. As it has been scheduled in Table 1, simulations in studying the effect of interfacial tension in laboratory situation ($\Re_1$) and full-scale oil-spill situation ($\Re_2$) have been carried out

in this section of the study.

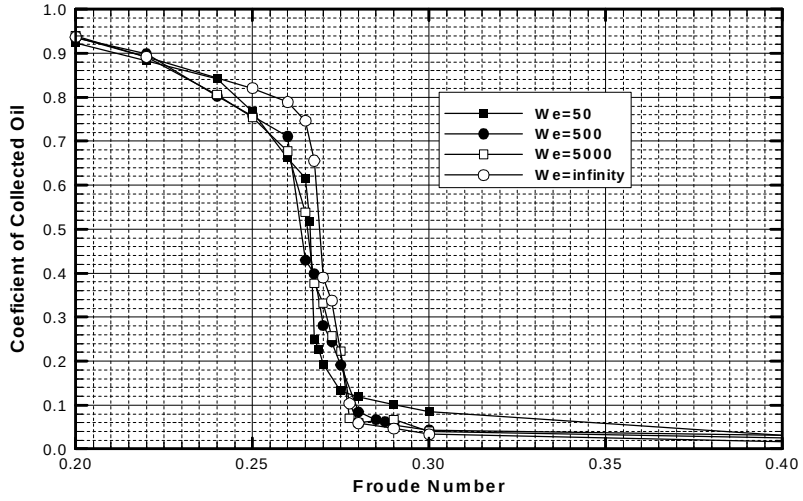

Figure 11 Effect of the Weber number (the first parameter set)

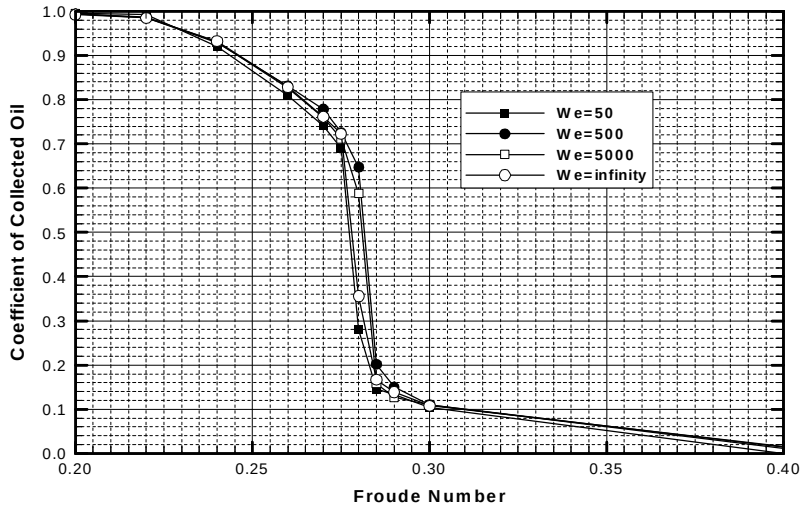

Figure 12 Effect of the Weber number (the second parameter set)

From the simulations, it is found that the oil-water interface shape is substantially influenced by the value of Weber number: the smaller the Weber number, the smoother the interface shape. With $We = 50$, the oil slick stays intact over the water layer. The interface is smooth and flat. Only a little water enters the oil

slick. With the increase of the Weber number, more and more water is mixed with the oil slick, and the interface behind the headwave becomes more irregular. If the computational cells are finer than the small oil droplets generated by the mechanism of Kelvin-Helmholtz instability, small oil droplets may be found in the simulations. Even with the present grid system, oil droplets are still found in some calculations. But the oil droplets in the present simulations are large; they have a better chance of being brought back to the oil slick via buoyancy than the Kelvin-Helmholtz droplets. This may partially explain the results presented in Fig. 11 and Fig. 12. The coefficients of collected oil are very close regardless of the value of the Weber number studied, even though the interfacial tension has a substantial influence on the shape of the oil-water interface. Fig. 11 and Fig. 12 summarize the results. The range of $F_{cr}^{\Re_1 \setminus \{We\}+\{We\}}$ is [0.263, 0.269], and the range of $F_{cr}^{\Re_2 \setminus \{We\}+\{We\}}$ is [0.275, 0.280]. The differences of the critical Froude numbers are only 0.006 and 0.005, respectively.

4.3 Effect of the Depth Ratio

According to Ertekin and Sundararaghavan's numerical study (1995) which was done in one-fluid model, the disadvantageous pressure gradient near an oil boom increases when the depth ratio decreases. From this fact, Ertekin and Sundararaghavan found that the instability of an oil slick contained by an oil boom should be very much dependent on the depth ratio.

In this section, we will use our "two-fluid" model to investigate the relationship between the critical Froude number and the depth ratio. From these two figures, it is found that the critical Froude number varies by 0.153 for the first condition with the parameter set $\Re_1 \setminus \{h_d\} + \{h_d\}$, and by 0.132 for the second condition with the

parameter set $\Re_2 \setminus \{h_d\} + \{h_d\}$. It is obtained from the previous two sections that the critical Froude number varies by only 0.1 when the oil relative viscosity changes and by only 0.06 when the Weber number changes. Based on the study of the parameter sets presented, it may be concluded that the depth ratio is a more important factor than the oil relative viscosity and the Weber number, if depth ratio is less than 10.

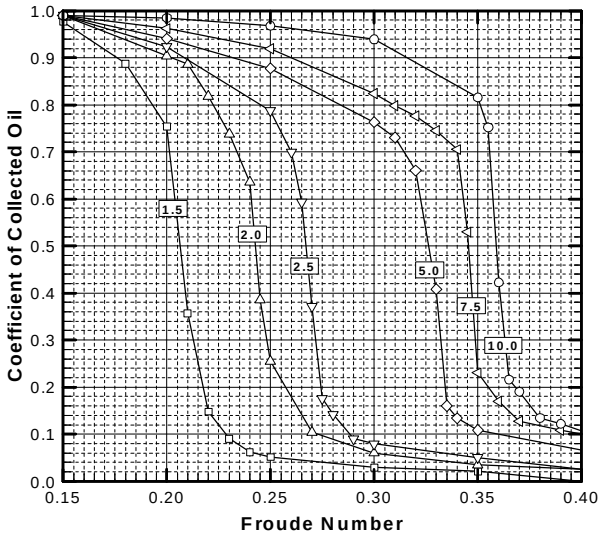

Figure 13 Effect of the depth ratio (the first parameter set)

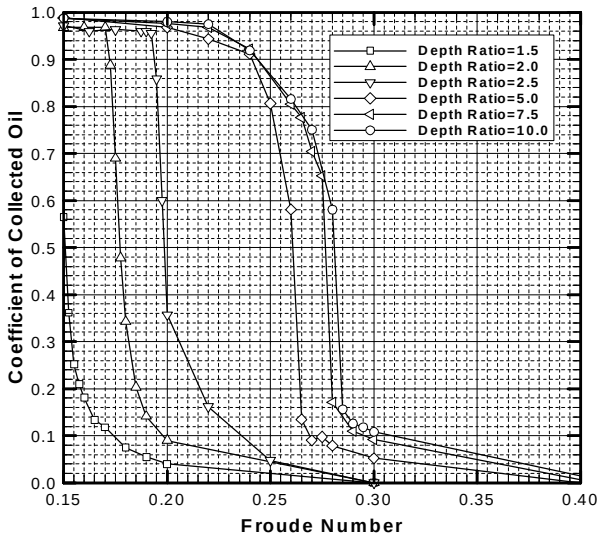

Figure 14 Effect of the depth ratio (the second parameter set)

The plot of the critical Froude number vs. the depth ratio is drawn in Fig. 15. It is found that when the depth ratio increases, the critical Froude number increases. But the rate of increase decreases monotonously. Suppose that the rate of increase is 1 at $h_d = 1.5$, then it is only 0.04 at $h_d = 10.0$ for the first condition and 0.05 for the second. With the best exponential fit, the rates of increase obtained are such that,

$$\left.\begin{aligned} \frac{dF_{cr}^{\Re_1 \setminus \{h_d\}+\{h_d\}}}{dh_d} &\propto e^{-0.437 h_d} \\ \frac{dF_{cr}^{\Re_2 \setminus \{h_d\}+\{h_d\}}}{dh_d} &\propto e^{-0.443 h_d} \end{aligned}\right\} \tag{28}$$

It is reasonable to assume that the rate of increase has the following general expression,

$$\frac{dF_{cr}^{\Re \setminus \{h_d\}+\{h_d\}}}{dh_d} \propto e^{-0.44 h_d} \tag{29}$$

Thus, in the range of $h_d \in [1.5, 10]$, the relationship between the critical Froude number and the depth ratio can be formulated as

$$\mathrm{F}_{cr}^{\Re\setminus\{h_d\}+\{h_d\}} = a_0 e^{-0.44 h_d} + b_0 \tag{30}$$

For the first condition, the constants are $a_0 = -0.303$, and $b_0 = 0.362$, and for the second condition, the constants are $a_0 = -0.261$, and $b_0 = 0.285$. When the depth ratio reaches infinity, $\mathrm{F}_{cr}^{\Re\setminus\{h_d\}+\{h_d\}} = b_0$. This value is very close to the critical Froude number at $h_d = 10$, which is equal to 0.358 for the first condition and 0.282 for the second condition, respectively. This implies that when the $h_d > 10$, the influence of the depth ratio can be neglected, and the infinite depth model may be applied.

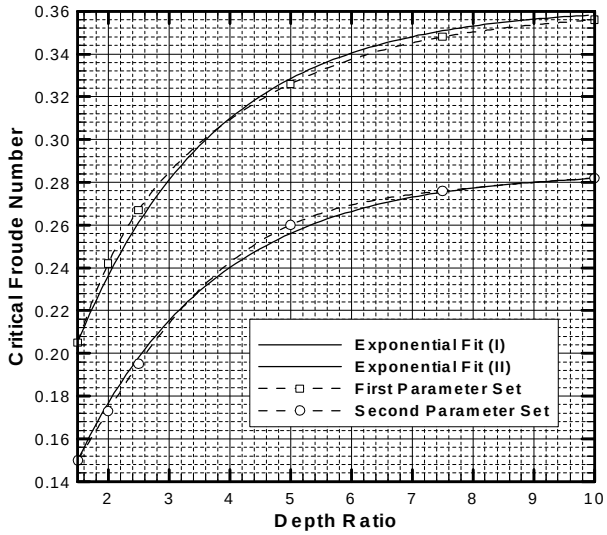

Figure 15 Critical Froude number vs. the depth ratio

4.4 Effect of the Oil Relative Density

In real oil spills, the densities of most crude oils are very close to the density of water, with the oil relative density $0.9 \le s_r < 1$. While in most of the laboratory

studies, the light oils (engine oils, kerosene, *et al.*) with $0.80 < s_r < 0.90$ are commonly used. To predict the instability of the real-life oil slicks from the results obtained from the light-oil laboratory experiments, it is necessary to investigate the behaviors of oil slicks with different densities. In the calculations presented in this section, four different oil relative densities, 0.80, 0.85, 0.90 and 0.95 are selected to study for this purpose.

As shown in Figures 16 and 17, the critical Froude numbers are varied in a large range with these four oil relative densities. As we know, it is the buoyancy force that keeps the oil separate from water. The lower the oil density, the greater the buoyancy force. The dimensionless form of the buoyancy force can be expressed as the reduced gravity:

$$g_r = \frac{1 - s_r}{\mathrm{Fr}^2} \tag{31}$$

Kordyban (1990, 1992) used the reduced gravity as the instability criterion to present the kerosene experiment results, and Ertekin and Sundararaghavan (1995) analyzed the experimental data extracted from Kordyban (1990) and Wicks (1969). The values of the critical reduced gravity (corresponding to the critical Froude number) were found in the range of $[1, 6]$.

The plots of Fig. 16 and Fig. 17 are redrawn into Fig. 18 with one changed variable: the reduced gravity takes place of the Froude number.

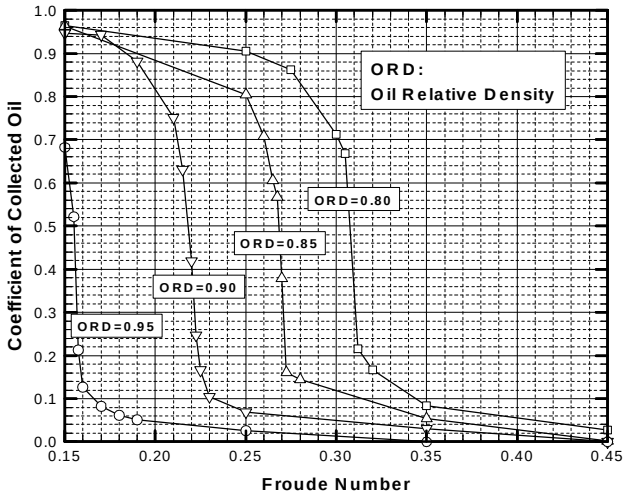

Figure 16 Effect of the oil relative density (the first parameter set)

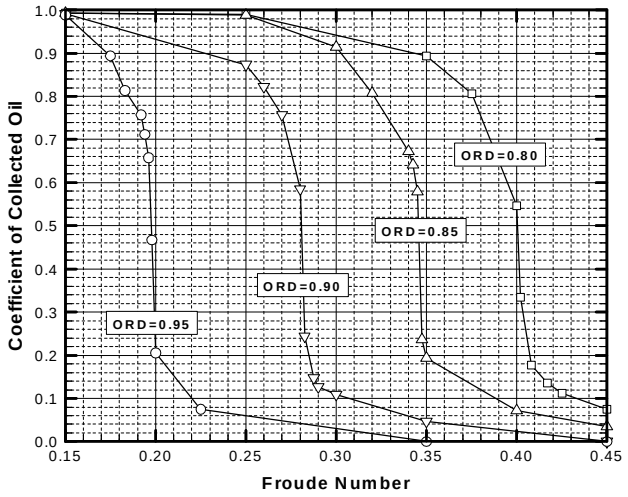

Figure 17 Effect of the oil relative density (the second parameter set)

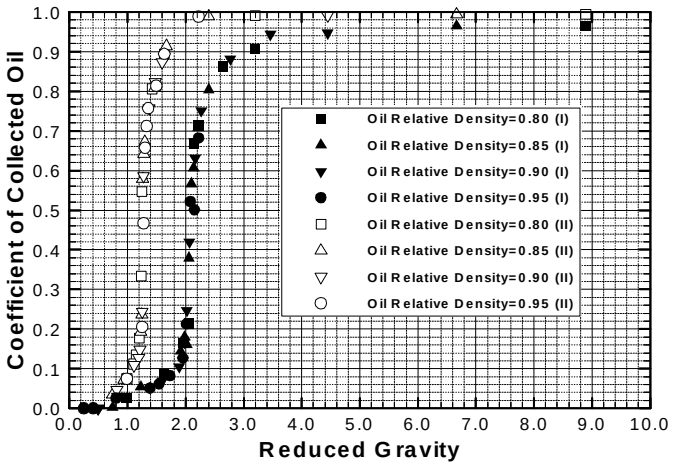

Figure 18 Coefficient of collected oil vs. the reduced gravity

In Fig. 18, it is observed that each set of four plots in Fig. 16 and Fig. 17 merges into one; different oil relative densities make no difference in the relationship between the coefficient of collected oil and the reduced gravity. This result strongly supports the fact that the reduced gravity is a more meaningful parameter than the Froude number in the study of the oil-spill instability. The critical reduced gravity is around 2.1 for the cases with the first parameter set and 1.2 for those with the second parameter set. Both of them are in the range of [1,6].

4.5 Effect of the Reynolds number

By studying the experimental data extracted from Kordyban (1990) and Wicks (1969), Ertekin and Sundararaghavan (1995) found that the critical reduced gravity depends less on the Reynolds number as Reynolds number becomes large. While at lower Reynolds number, the experimental data suggests an inverse dependence between the critical reduced gravity and the Reynolds number.

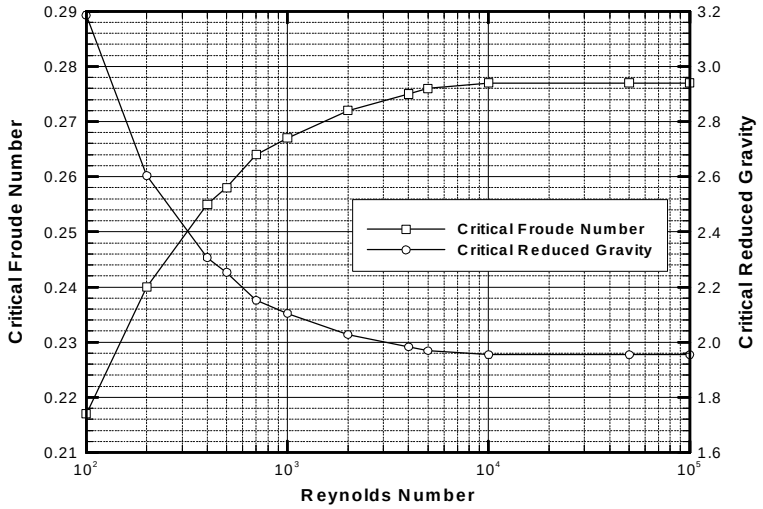

Figure 19 Effect of the Reynolds number

To numerically study the effect of the Reynolds number, about 150 cases with parameter set $\Re_1 \setminus \{\mathrm{Re}\}$ and 12 different Reynolds numbers have been calculated. The results are summarized in Fig. 19, presented as the plots of the Reynolds number vs. both the critical Froude number and the critical reduced gravity. From Fig. 19, it is seen that the critical reduced gravity does have an approximately inverse dependence on the Reynolds number in the logarithmic scale for the range of $\mathrm{Re} < 10^4$; when $\mathrm{Re} > 10^4$, the critical reduced gravity no longer varies with the Reynolds number. These results agree qualitatively with the results provided by the aforementioned references.

Fundamentally, the buoyancy is the ultimate force to prevent an oil slick from escaping, so it is always important. The reduced gravity (g_r) is the dimensionless form of buoyancy, scaled by the inertia force, and the inverse of the Reynolds number ($1/\mathrm{Re}$) is the measurement of the viscous force also scaled by the inertia force. If the viscous effect is as important as the buoyancy, then, physically g_r and $1/\mathrm{Re}$ should

be in the same order, $g_r \sim 1/\mathrm{Re}$.

In real situations, the reduced gravity is larger than 1, and the Reynolds number is larger than 1000. Then $g_r >> 1/\mathrm{Re}$. So there is only a weak relationship between the reduced gravity and the Reynolds number, even for Reynolds number in the low range ($10^2 \le \mathrm{Re} \le 10^3$). When the Reynolds number increases, the viscous effect ($O(1/\mathrm{Re})$) becomes weaker, finally it may be negligible ($1/\mathrm{Re} \to 0$), while the reduced gravity is usually in the order of 1. This is the reason that the critical reduced gravity is independent of the Reynolds number when the Reynolds number is very large.

5 Conclusions

In this study, we have numerically investigated the drainage failure and the critical accumulation failure. Given the present numerical model and parameter sets, the simulations suggest that:

(a) The vortices in an oil slick with low relative viscosity ($s_m < 1000$) allow the whole slick to be stable, but a strong vortex may break the slick into oil droplets, which may then contribute to entrainment failure. In a highly viscous oil slick ($s_m > 2000$), the large oscillations cause the slick to escape easily under a single boom. The oil slick with a relative oil viscosity $s_m \approx 100$ is the most stable slick in this class of study.

(b) In drainage failure and critical accumulation failure, the contribution from the oil-water interfacial tension may be negligible.

(c) When $h_d < 10$, the depth ratio has a significant effect on the critical instability

criteria. The smaller the depth ratio, the smaller the critical Froude number. When $h_d > 10$, the infinite depth approach is acceptable with reasonable accuracy.

(d) The coefficient of collected oil drops quickly at a certain Froude number. This distinguishing feature makes the Froude number a good parameter to determine the critical containment condition. The reduced gravity naturally combines the effects of the Froude number and the oil density. As a criterion, the reduced gravity is more appropriate than the Froude number.

(e) When $\mathrm{Re} < 10^4$, the critical reduced gravity is weakly and inversely proportional to the Reynolds number. When $\mathrm{Re} > 10^4$, the critical reduced gravity is independent of the Reynolds number.

References

Bai, K.J. and Kim, J.W., "A computational model for flow around an oil boom", Proceedings of Workshop on Tidal and Oil Spill Modeling 1993; 5-17

Brackbill, J.U., Kothe, D.B. and Zemach, C., "A continuum method for modeling surface tension", Journal of Computational Physics 1992; 100: 335-354

Clavelle, E. J. and Rowe, R. D., "Numerical simulation of oil-boom failure by critical accumulation", Arctic Marine Oil Spill Program Technical Seminar 1993; 409-418

Cross, R.H. and Hoult, D. P., "Oil booms in tidal currents", Proceedings of 12th Coastal Engineering Conference, ASCE 1970; 1745-1758

Delvigne G.A.L., "Barrier failure by critical accumulation of viscous oil", Proceedings of Oil Spill Conference, USEPA, USCG, and American Petroleum Institute 1989; 143-148

Ertekin, R. C., Sundararaghavan, H., “The calculations of the instability criterion for a uniform viscous flow past an oil boom”, Journal of offshore mechanics and Arctic engineering 1995; 117: 24-29

Fang, J. Z., Instability Study of Oil Slicks Contained by Oil Boom Systems, Ph.D. Dissertation, University of Miami, 2000.

Fang, J.Z. and Wong, K. V., “An advanced VOF algorithm for oil boom design”, International Journal of Environmental Pollution (Accepted), 1999.

Grilli, S.T., Hu, Z., Spaulding, M.L., “A hydrodynamic model of oil containment by a boom: Phase I”, Final Technical Report, University of Rhode Island, 1996.

Grilli, S.T., Hu, Z., Spaulding, M.L., and Liang, D., “Numerical modeling of oil containment by a boom/barrier system: Phase II”, Final Technical Report, University of Rhode Island, 1997.

Johnston, A.L., Fitzmaurice, M.R. and Watt, R.G.M., “Oil spill containment: viscous oils”, Proceedings of Oil Spill Conference, USEPA, USCG, and American Petroleum Institute, 1993; 89-94

Kordyban, E., “The behavior of the oil-water interface at a planar boom”, Journal of Energy Resources Technology 1990; 112: 90-95

Kordyban, E., “The effect of waves on the oil slick at a retention boom”, Journal of Energy Resources Technology 1992; 114: 31-37

Leibovich, S., “Oil slick instability and the entrainment failure of oil containment booms”, Journal of Fluids Engineering 1976; 98: 93-108

Milgram, J.H, Van Houten, R.J., “Mechanics of a restrained layer of floating oil above a water current”, Journal of Hydronautics 1978; l12: 93-108

Puckett, E.G., Almgren, A.S., “A high-order projection method for tracking fluid interfaces in variable density incompressible flows”, Journal of Computational Physics 1997; 130: 269-282

Wicks, M. IV, “Fluid dynamics of floating oil containment by mechanical barriers in the presence of water currents”, Proceedings API-FWPCA Joint Conference on Prevention and Control of Oil Spills, New York 1969; 55-106

Zalosh, R.G., Jensen, D.S., “A numerical model of droplet entrainment from a contained oil slick”, Fluid Mechanics in the Petroleum Industry, ASME, 1975; 17-27

Zalosh, R.G., “Discretized simulation of vortex sheet evolution with buoyancy and surface tension effects”, AIAA Journal 1976; 14(11): 1517-1523